ChemComm

COMMUNICATION

View Article Online
View Journal | View Issue

Cite this: *Chem. Commun.*, 2021, **57**, 12772

Received 13th September 2021,
Accepted 9th November 2021

DOI: 10.1039/d1cc05144j

rsc.li/chemcomm

Inexpensive gram scale synthesis of porous Ti_4O_7 for high performance polymer electrolyte fuel cell electrodes†

Mitsuharu Chisaka,*[a] Waka Nagano,*[b] Byambasuren Delgertsetseg*[b] and Tatsuya Takeguchi*[b]

As a fuel cell catalyst support, more than 2 g of Magnéli phase Ti_4O_7 fine-particles were synthesized in a single reaction *via* an inexpensive route. The single-cell performance reached that of commercial carbon-supported platinum, with an excellent load cycle durability, one of the highest ever reported for oxide-supported platinum catalysts.

Following the commercialization of polymer electrolyte fuel cell (PEFC)-powered passenger vehicles in the 2010s, they remain a niche market despite the longer travel distances (>500 km) and higher power density compared with battery-driven electric vehicles.[1] The high cost of platinum-based catalysts has been assumed to present the highest barrier to widespread use.[2] Currently, platinum-based nanoparticle catalysts are supported on conductive carbon black to maximize the "active" platinum surface area where the three reactants, *i.e.* gases, protons, and electrons, can access the platinum surface simultaneously. Carbon black is an excellent support material, delivering: (1) a high Brunauer–Emmett–Teller surface area, S_{BET}, of above 100 $m^2\ g^{-1}$; and (2) high electrical conductivity, σ, of above 1 S cm^{-1} at low compression pressures, typically below 10 MPa. The low cost is another advantage, although additional costs are required to protect the material from oxidation.[3] Several oxide materials, including titanium dioxides,[4,5] titanium suboxides,[6,7] and tin dioxides,[8,9] have been developed as support materials because they are stable in PEFC cathodes, where four times higher platinum loading is currently needed compared with the anodes.[10] However, both the S_{BET} and σ values of the oxides are generally insufficient; the values are often one or even two orders of magnitude lower than those of carbon black, reducing the cell performance. Recently, He *et al.* successfully prepared antimony-doped tin dioxide with an exceptionally high σ of 6.2 S cm^{-1} without disclosing the compression pressure, while the S_{BET} was below 50 $m^2\ g^{-1}$.[9] The preparation of oxide supports exceeding both thresholds (1) and (2) is a major challenge. Magnéli phase titanium suboxides, with a composition that can be expressed as Ti_nO_{2n-1}, are well known as conductive oxides with a maximum σ at $n = 4$.[11] The highest S_{BET} of a Ti_4O_7 support for PEFCs remains low, at 26 $m^2\ g^{-1}$.[7] In this study, fine Ti_4O_7 particles were synthesized as supports in an attempt to meet these challenging targets. The particles were synthesized from titanium oxysulfate ($TiOSO_4$) and polyethylene glycol with an average molecular weight of 360–440 (PEG400) *via* a carbothermal reduction reaction. This route was originally reported by the Nazar group, and uses conductive Ti_4O_7 as a lithium sulfur battery cathode, with the Ti_4O_7 synthesized from titanium ethoxide and PEG400.[12] We selected $TiOSO_4$ as it is stable in air and easy to handle, making it more suited to the mass production of Ti_4O_7 than titanium ethoxide or other titanium sources that react readily with moisture in the air. The details of the catalyst synthesis and characterization are described in S1 and S2, ESI.†

After optimizing the precursor composition and annealing conditions (S3, ESI†), fine Ti_4O_7 particles were synthesized as shown in Fig. 1(a). Submicron particles formed aggregates with a broad pore size distribution (S4, ESI†). Magnéli phase Ti_4O_7 is generally synthesized at higher temperatures, typically 1323 K or above, and for much longer durations.[13] The PEG400-derived carbon species produced a reductive atmosphere and thus the annealing temperature and duration were successfully suppressed to 1240 K and 3 h, respectively, yielding a high S_{BET} of 172 $m^2\ g^{-1}$. When commercial TiO_2 powders were annealed under the flow of an identical gas mixture, 10% v/v H_2/Ar, a higher temperature of 1323 K and longer duration of 6 h was needed to obtain much larger particle sizes of Ti_4O_7 powders, Ti_4O_7-L, as shown in Fig. 1(b). The composition can be easily

[a] *Department of Sustainable Energy, Hirosaki University, 3 Bunkyo-cho, Hirosaki, Aomori 036-8561, Japan. E-mail: chisaka@hirosaki-u.ac.jp*
[b] *Faculty of Science and Engineering, Iwate University, 4-3-5 Ueda, Morioka, Iwate 020-8551, Japan. E-mail: wnagano@iwate-u.ac.jp, delgerts@iwate-u.ac.jp, takeguch@iwate-u.ac.jp*

† Electronic supplementary information (ESI) available: Experimental details, elemental analyses, pore size distributions, XRD patterns, FE-SEM images, XP spectra and RDE voltammograms. See DOI: 10.1039/d1cc05144j

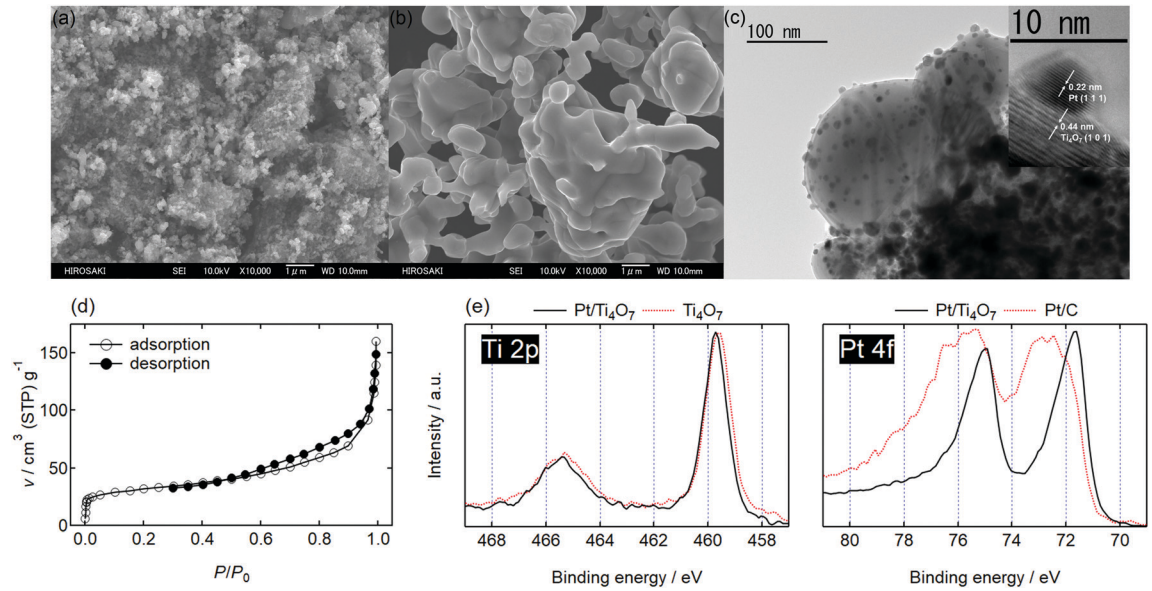

Fig. 1 Field emission-scanning electron microscopy (FE-SEM) images of (a) Ti_4O_7 particles synthesized from titanium oxysulfate/polyethylene glycol mixture and (b) Ti_4O_7 powders synthesized from commercial TiO_2, Ti_4O_7-L. (c) A transmission electron microscopy (TEM) image, (d) an N_2 adsorption/desorption isotherm, and (e) Ti 2p and Pt 4f X-ray photoelectron (XP) spectra of 20% w/w Pt/Ti_4O_7 catalyst. The inset in (c) shows the high-resolution TEM (HR-TEM) image. For reference, a Ti 2p spectrum of Ti_4O_7 and a Pt 4f spectrum of commercial Pt/C are shown by the dashed curves in (e).

controlled to yield the further reduced Ti_3O_5 and Ti_2O_3 phases by controlling the annealing temperature and starting material of the present carbothermal reduction route, respectively (S3, ESI†). The batch size, *i.e.*, the mass of Ti_4O_7 per annealing, was also easily increased to more than 2 g by simply increasing the mass of the precursor mixture (S3, ESI†).

Platinum nanoparticles were supported on the Ti_4O_7 particles using a recently reported ethanol reduction method.[14] The transmission electron microscopy (TEM) images of 20% w/w Pt/Ti_4O_7 are shown in Fig. 1(c). Platinum particles of less than 10 nm in diameter were highly dispersed on the Ti_4O_7 support. The HR-TEM image shown in the inset indicates that platinum nanoparticles were in direct contact with the Ti_4O_7 particles. The N_2 adsorption–desorption isotherm is displayed in Fig. 1(d). A type IIb isotherm with a H3 hysteresis loop was observed according to the classification by Rouquerol *et al.*[15] and no plateau appears at a high relative pressure, P/P_0. It is a typical isotherm for porous materials in which pores originate from the space between aggregates;[15,16] in this case, the aggregates were composed of the fine Pt/Ti_4O_7 particles.

The surface chemical states of the Pt/Ti_4O_7 catalysts were investigated using X-ray photoelectron spectroscopy (XPS) and their Ti 2p and Pt 4f spectra are displayed in Fig. 1(e). The Ti 2p and Pt 4f core levels split into Ti $2p_{3/2}$/Ti $2p_{1/2}$ and Pt $4f_{7/2}$/Pt $4f_{5/2}$, as shown by doublets in the spectra. The Ti_4O_7 supports displayed a Ti $2p_{3/2}$ peak at approximately 459 eV in Fig. 1(e), which was assigned to Ti^{4+} in TiO_2.[17] No clear peaks from Ti^{3+} were observed in the Ti 2p spectrum of Ti_4O_7, indicating that the surface of Ti_4O_7 was oxidized to form a thin layer of TiO_{2-x}.[6] The corresponding Raman spectrum showed rutile TiO_2 with oxygen vacancies (S3, ESI†), and agreed well with these XPS analyses. The Hwang group also reported that the Ti_4O_7 surface was oxidized to form a rutile TiO_2 layer.[18] The Ti $2p_{3/2}$ peak shifted to higher binding energy regions after platinum nanoparticles were supported, as shown in Fig. 1(e), indicating that the electron density of titanium decreased. The Pt 4f spectrum of Pt/Ti_4O_7 showed lower Pt $4f_{7/2}$ peak binding energy compared with that of commercial Pt/C, indicating that the electron density of platinum nanoparticles was higher in Pt/Ti_4O_7 than Pt/C. The Ti 2p and Pt 4f spectra presented in Fig. 1(e) indicate that the electrons from the titanium atoms in Ti_4O_7 supports were transferred to the platinum atoms. These results were in good agreement with previous oxide-supported platinum catalysts, in which strong metal–support interactions (SMSIs) were reported to enhance oxygen reduction reaction (ORR) activity.[19] The SMSI was enhanced by increasing platinum fraction, w_{Pt} (S5, ESI†).

Both the platinum particle size, d_{Pt}, and the chemically active surface area of platinum nanoparticles in Pt/Ti_4O_7, S_{CSA}, were evaluated using a CO pulse method and the electrochemically active platinum surface area, S_{ECSA}, was evaluated using CO stripping voltammetry. The results are summarized in Table 1. As w_{Pt} decreased, d_{Pt} decreased and S_{CSA} increased, indicating that the platinum nanoparticles were highly dispersed on Ti_4O_7. Indeed, the corresponding XRD peaks were too broad to calculate the crystallite size when $w_{Pt} < 20\%$ w/w (S6, ESI†). The S_{ECSA} displayed a similar trend to w_{Pt} when compared with S_{CSA}, indicating that the protons and electrons could access the surface of small platinum nanoparticles. At $w_{Pt} = 5\%$ w/w, S_{ECSA} was larger than S_{CSA} suggesting the presence of small platinum particles which were insensitive to the CO pulse method. These Pt/Ti_4O_7 catalysts exhibited

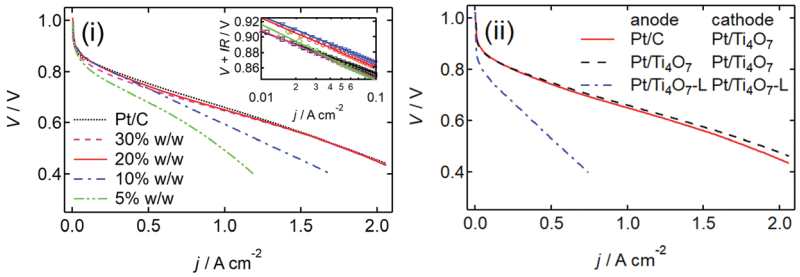

Fig. 2 (i) $j - V$ curves of five membrane electrode assemblies (MEAs) fabricated using 46% w/w Pt/C and Pt/Ti_4O_7 with four different platinum fractions, w_{Pt}, of 5%, 10%, 20%, and 30% w/w in the cathode. The Pt/C was used in the anode of all MEAs. (ii) j–V curves of three MEAs fabricated using Pt/C in the anode and 20% w/w Pt/Ti_4O_7 in the cathode, 20% w/w Pt/Ti_4O_7 in both the anode and the cathode, and 20% w/w platinum on Ti_4O_7 powder as shown in Fig. 1(b), Pt/Ti_4O_7-L in both the anode and cathode. The platinum loading at the anode and cathode was at 0.2 and 0.5 mg_{Pt} cm^{-2}, respectively.

excellent ORR activity in a single cell cathode, as shown in Fig. 2(i). Membrane electrode assemblies (MEAs) were fabricated using commercial Pt/C at the anode and Pt/Ti_4O_7 or Pt/C at the cathode, and then the current density *versus* voltage (j–V) curves were obtained at 353 K. These curves were separately interpreted at $V \geq 0.8$ V and $V < 0.8$ V. At $V \geq 0.8$ V, the curves were analyzed using eqn (1) to reveal the ORR kinetics in a single cell:[20]

$$V = V^0 - b\log(j) - jRA \quad (1)$$

where $V^0 = V^r + b\log(j_0)$, V^r (V) is the reversible cell voltage, b (V dec^{-1}) is the Tafel slope, j_0 (mA cm^{-2}) is the exchange current density for ORR, R (Ω) represents the resistance including the ohmic losses and the diffusion losses in both the gas phase and thin Nafion films covering the Pt/Ti_4O_7 or Pt/C, and A is the catalyst layer area, 4.84 cm^2. As b changes at approximately $V = 0.8$ V,[21] only the data at $V \geq 0.8$ V were analyzed. The results of the least-squares fitting of eqn (1) to those data shown in the inset of Fig. 2(i) are summarized in Table 1. Although S_{ECSA} monotonously increased with a decrease in w_{Pt}, V^0 was similar at $w_{Pt} \leq 20\%$ w/w, indicative of the similar activation losses. These different trends in S_{ECSA} and V^0 could be from the difference in a half cell and a single cell; protons were abundant in the former in which aqueous 0.1 mol dm^{-3} $HClO_4$ electrolyte was utilized whereas protons should be transported across the catalyst layer composed of Nafion and Pt/Ti_4O_7 in the latter. When w_{Pt} decreased at a constant platinum loading, the catalyst layer thickness increased to increase the ohmic loss; thus, the active surface area was formed only near the membrane side at lower w_{Pt}. Indeed, RA increased significantly with a decrease in w_{Pt}, indicating the increased thickness. As b values were similar at around 0.06 V $decade^{-1}$, which is typical of platinum,[21] except for 5% w/w Pt/Ti_4O_7, the ORR proceeded under a similar mechanism in Pt/Ti_4O_7 with $w_{Pt} \geq 10\%$ w/w and Pt/C. The slightly larger b of 5% w/w Pt/Ti_4O_7 originates from the larger catalyst layer thickness, which restricts oxygen and proton transport, as they both increase b.[22] The mass activity, i_m, evaluated at $V + IR = 0.85$ V[8] was maximized at $w_{Pt} = 10\%$ w/w, resulting in 404 A g_{Pt}^{-1}. However, V dropped significantly at $V < 0.8$ V for $w_{Pt} \leq 10\%$ w/w owing to the high RA caused by the larger catalyst layer thickness at lower w_{Pt}. Therefore, the optimum w_{Pt} was 20% w/w and the performance was almost the same as that of commercial 46% w/w Pt/C. Then, an MEA was prepared using the optimum 20% w/w Pt/Ti_4O_7 for both the anode and cathode and the $j - V$ curves are shown in Fig. 2(ii). The performance was almost the same as that of the MEA with a Pt/C anode. The results from Fig. 2(i) and (ii) indicate that the optimum 20% w/w Pt/Ti_4O_7 catalyzed both the anode hydrogen oxidation reaction (HOR) and cathode ORR and that the HOR/ORR performances were similar to those of commercial Pt/C. When the large-sized Ti_4O_7-L powder shown in Fig. 1(b) was used as a support under identical conditions, much lower V was obtained at any j owing to the high ohmic loss, even after optimizing the platinum loading in both the anode and cathode (S7, ESI†); the maximum j was only 0.74 A cm^{-2}, as shown by a dash-dotted curve in Fig. 2(ii). Further, the V^0 of the MEA employing Pt/Ti_4O_7-L was much lower than that of other MEAs, as shown in Table 1, indicating that a small active surface area was formed in the catalyst layer with Pt/Ti_4O_7-L as the platinum particles located near the gas diffusion layer side could not be utilized and ORR occurs only on those near the membrane side in the thicker catalyst layers.[23] The single-cell performance delivered from the current Pt/Ti_4O_7 particles displayed by the dashed curve in

Table 1 Platinum particle size, d_{Pt}, and chemically active platinum surface area, S_{CSA}, both obtained using a CO pulse method, electrochemically active platinum surface area obtained using CO stripping voltammetry, S_{ECSA}, and kinetic parameters obtained from the least squares fitting of eqn (1) to current density *versus* cell voltage (j–V) curves at $V \geq 0.8$ V in Fig. 2(i) and (ii)

Catalyst	d_{Pt} (nm)	S_{CSA} (m^2 g_{Pt}^{-1})	S_{ECSA} (m^2 g_{Pt}^{-1})	V^0 (V)	b (V dec^{-1})	RA (Ω cm^2)	i_m (A g_{Pt}^{-1})
30% w/w Pt/Ti_4O_7	6.8	40.8	32.7	0.970 ± 0.000	0.061 ± 0.000	0.146 ± 0.001	185
20% w/w Pt/Ti_4O_7	4.2	66.0	58.2	0.983 ± 0.001	0.059 ± 0.001	0.157 ± 0.002	351
10% w/w Pt/Ti_4O_7	3.4	82.0	116.0	0.986 ± 0.001	0.059 ± 0.000	0.172 ± 0.001	404
5% w/w Pt/Ti_4O_7	2.1	131.6	210.9	0.985 ± 0.009	0.074 ± 0.005	0.222 ± 0.023	166
46% w/w Pt/C	N/A	N/A	88.3	0.961 ± 0.001	0.053 ± 0.001	0.094 ± 0.003	245
20% w/w Pt/Ti_4O_7-L	N/A	N/A	N/A	0.926 ± 0.005	0.065 ± 0.004	0.347 ± 0.066	28

Fig. 2(ii) was at least partly responsible for the high σ of Ti_4O_7 particles, as shown in Fig. S10 (S7, ESI†). The σ exceeded 1 S cm^{-1} at a low compression pressure of 6 MPa, and the value was only one order of magnitude lower than that of the commercial carbon black, Ketjen black EC600JD, at any pressure. The small particle size increases the tensile strain, distorting the lattice and thereby increasing the number of oxygen vacancies. A large number of oxygen vacancies was introduced to the surface of small Ti_4O_7 particles (S3, ESI†) to enhance σ, which is known to be increased by the incorporation of oxygen vacancies.[24] The durability over the load cycles for vehicles is shown in Fig. S12 (S8, ESI†). The V did not change at any j after 10 000 cycles, indicating that neither HOR nor ORR performance changed over the 10 000 cycles. Commercial SnO_2-supported platinum displayed much lower durability. In Table S1 (S8, ESI†), the load cycle durability of platinum or platinum–cobalt supported on oxide catalysts reported to date is summarized. The changes in V at j = 1.0 A cm^{-2} during the cycles, which was previously utilized by Ramani group,[5] were used as a measure of durability as high loads are needed in vehicles. The load cycle durability of the present Pt/Ti_4O_7 is among the highest of the state-of-the-art Pt/oxide catalysts,[4,5,8,9] indicating that Ti_4O_7 stabilized the platinum nanoparticles well. Although the mechanism is still under investigation, one of the reasons may be the SMSI, as platinum nanoparticles are in contact with Ti_4O_7 with a large surface area; a S_{BET} close to normal carbon black and among the highest in oxide supports reported to date, 172 m^2 g^{-1}.

In summary, Magnéli phase Ti_4O_7 particles were synthesized *via* carbothermal reduction to yield high σ and S_{BET} values of 1.2 S cm^{-1} at low compression pressure (6 MPa) and 172 m^2 g^{-1}, respectively. The precursors are low-cost, stable in air, and easy to handle and to increase the mass of Ti_4O_7; more than 2 g were synthesized at once. The resulting Ti_4O_7 particles supported the platinum nanoparticles to display SMSI between the platinum and Ti_4O_7. The optimized 20% w/w Pt/Ti_4O_7 exhibited excellent HOR/ORR performances in a single cell, almost the same as those of commercial Pt/C. The load cycle durability was the highest among the state-of-the-art platinum/oxide catalysts, with no change in the cell performance after 10 000 voltage cycles.

Mitsuharu Chisaka worked on conceptualization, support synthesis, physical and chemical characterizations, data curation, formal analysis, funding acquisition, investigation, writing (original draft), and writing (review & editing). Waka Nagano worked on catalyst synthesis, elemental analyses, preparation of MEAs, and single cell tests. Byambasuren Delgertsetseg worked on the CO pulse experiments and CO stripping voltammetry. Tatsuya Takeguchi worked on methodology, funding acquisition, investigation, and writing (review & editing).

We thank Mr Yusei Tsushima at Hirosaki University and Ms Kyoko Mitsunari at Horiba Techno Service Co., Ltd for performing FE-SEM/TEM imaging and particle size analyses, respectively. This work was partially supported by a grant from the New Energy and Industrial Technology Development Organization, Japan. Part of the work was conducted at the Advanced Characterization Nanotechnology Platform of the University of Tokyo, supported by the ''Nanotechnology Platform'' of the Ministry of Education, Culture, Sports, Science and Technology in Japan, grant number JPMXP09A21UT0016.

Conflicts of interest

There are no conflicts to declare.

Notes and references

1 O. Gröger, H. A. Gasteiger and J. P. Suchsland, *J. Electrochem. Soc.*, 2015, **162**, A2605.
2 M. M. Whiston, I. L. Azevedo, S. Litster, K. S. Whitefoot, C. Samaras and J. F. Whitacre, *Proc. Natl. Acad. Sci. U. S. A.*, 2019, **116**, 4899.
3 U. Eberle and R. von Helmolt, *Energy Environ. Sci.*, 2010, **3**, 689.
4 (*a*) S. Y. Huang, P. Ganesan and B. N. Popov, *Appl. Catal., B*, 2011, **102**, 71; (*b*) A. Pătrua, A. Rabis, S. E. Temmel, R. Kotz and T. J. Schmidt, *Catal. Today*, 2016, **262**, 161; (*c*) P. Dhanasekaran, S. V. Selvaganesh and S. D. Bhat, *New J. Chem.*, 2017, **41**, 13012.
5 (*a*) A. Kumar and V. Ramani, *ACS Catal.*, 2014, **4**, 1516; (*b*) J. Parrondo, T. Han, E. Niangar, C. Wang, N. Dale, K. Adjemian and V. Ramani, *Proc. Natl. Acad. Sci. U. S. A.*, 2014, **111**, 45.
6 T. Ioroi, H. Kageyama, T. Akita and K. Yasuda, *Phys. Chem. Chem. Phys.*, 2010, **12**, 7529.
7 C. Yao, F. Li, X. Li and D. Xia, *J. Mater. Chem.*, 2012, **22**, 16560.
8 C. Takei, R. Kobayashi, Y. Mizushita, Y. Hiramitsu, K. Kakinuma and M. Uchida, *J. Electrochem. Soc.*, 2018, **165**, F1300.
9 C. He, X. Wang, S. Sankarasubramanian, A. Yadav, K. Bhattacharyya, X. Liang and V. Ramani, *ACS Appl. Energy Mater.*, 2020, **3**, 5774.
10 A. Kongkanand and M. F. Mathias, *J. Phys. Chem. Lett.*, 2016, **7**, 1127.
11 J. R. Smith, F. C. Walsh and R. L. Clarke, *J. Appl. Electrochem.*, 1998, **28**, 1021.
12 Q. Pang, D. Kundu, M. Cuisinier and L. F. Nazar, *Nat. Commun.*, 2014, **5**, 4759.
13 F. C. Walsh and R. G. A. Wills, *Electrochim. Acta*, 2010, **55**, 6342.
14 M. M. Rahman, K. Inaba, G. Batnyagt, M. Saikawa, Y. Kato, R. Awata, B. Delgertsetsega, Y. Kaneta, K. Higashide, T. Uruga, Y. Iwasawa, K. Ui and T. Takeguchi, *RSC Adv.*, 2021, **11**, 20601.
15 F. Rouquerol, J. Rouquerol, K. S. W. Sing, P. Llewellyn and G. Maurin, Adsorption by Powders and Porous Solids. Principles, *Methodology and Applications*, Academic Press, London, 2014, 2nd edn, p. 290.
16 (*a*) S. Abelló and J. Pérez-Ramírez, *Microporous Mesoporous Mater.*, 2006, **96**, 102; (*b*) G. S. Shao, F. Y. Wang, T. Z. Ren, Y. Liu and Z. Y. Yuan, *Appl. Catal., B*, 2009, **92**, 61.
17 (*a*) K. S. Robinson and P. M. A. Sherwood, *Surf. Interface Anal.*, 1984, **6**, 261; (*b*) N. C. Saha and H. G. Tompkins, *J. Appl. Phys.*, 1992, **72**, 3072.
18 A. D. Duma, Y. C. Wu, W. N. Su, C. J. Pan, M. C. Tsai, H. M. Chen, J. F. Lee, H. S. Sheu, V. T. T. Ho and B. J. Hwang, *ChemCatChem*, 2018, **10**, 1155.
19 I. Jiménez-Morales, F. Haidar, S. Cavaliere, D. Jones and J. Rozière, *ACS Catal.*, 2020, **10**(18), 10399.
20 M. Chisaka, E. Matsuoka and H. Daiguji, *J. Electrochem. Soc.*, 2010, **157**, B1218.
21 A. Parthasarathy, S. Srinivasan, A. J. Appleby and C. R. Martin, *J. Electrochem. Soc.*, 1992, **139**, 2530.
22 (*a*) Y. W. Rho, O. A. Velev, S. Srinivasan and Y. T. Kho, *J. Electrochem. Soc.*, 1994, **141**, 2084; (*b*) G. Li and P. G. Pickup, *J. Electrochem. Soc.*, 2003, **150**, C745.
23 M. Chisaka and H. Daiguji, *J. Electrochem. Soc.*, 2009, **156**, B22.
24 M. Zhang, Y. Wang, Y. Zhang, J. Song, Y. Si, J. Yan, C. Ma, Y. T. Liu, J. Yu and B. Ding, *Angew. Chem., Int. Ed.*, 2020, **59**, 23252.